Microfluid Nanofluid (2009) 6:241–251
DOI 10.1007/s10404-008-0320-6

RESEARCH PAPER

A Y-channel design for improving zeta potential and surface conductivity measurements using the current monitoring method

**Zeyad A. Almutairi · Tomasz Glawdel ·
Carolyn L. Ren · David A. Johnson**

Received: 23 April 2008 / Accepted: 30 May 2008 / Published online: 25 June 2008

Abstract This study presents a new Y-channel design for measuring the zeta potential and surface conductance of a solid-liquid pairing using the current monitoring technique. The new design improves the throughput and reliability of the testing apparatus since the displacement between two solutions can be repeated many times without interfering with the experiments. It also increases the accuracy of the measurement by producing sharper start and end transitions for the current–time plot of the solution displacement process. In this design, efforts have been made to minimize the effects of electrolysis, Joule heating and undesired pressure driven flow on the measurements. An improvement on the current–time slope analysis is also presented. The Y-channel design was validated by comparing zeta potential measurements to published results. The zeta potential of several biological buffers relevant to the microfluidic community in plasma treated PDMS/PDMS and PDMS/Glass microchannels are presented. Preliminary studies of surface conductivity measurements using the Y-channel design were also conducted and are briefly discussed.

Keywords Zeta potential ·
Current monitoring technique · Y-channel design ·
Current slope method · PDMS microchannel

Z. A. Almutairi · T. Glawdel · C. L. Ren (✉) · D. A. Johnson
Department of Mechanical and Mechatronics Engineering,
University of Waterloo, 200 University Avenue West,
Waterloo, ON N2L 3G1, Canada
e-mail: c3ren@mecheng1.uwaterloo.ca

1 Introduction

Electroosmotic flow (EOF) is widely used as a pumping method in a number of microfluidic applications such as micromixing (Zhang et al. 2006), cell sorting (Sun et al. 2007), electroosmotic pumps (Chen and Santiago 2002), and sample handling and separation (Fluri et al. 1996; Gravesen et al. 1993; Harrison et al. 1992) since it is simple to integrate and provides flexible control over multiple fluid streams. This flow phenomenon occurs when an externally applied electric field causes a net motion of mobile ions in the electric double layer (EDL) generating fluid flow through viscous drag. The fluid velocity varies only in the EDL, from zero at the wall to a maximum at the edge of the EDL given by the Helmholtz-Smoluchowski slip velocity (Masliyah and Bhattacharjee 2006):

$$u_{\text{slip}} = -\frac{\varepsilon_{\text{r}}\varepsilon_{\text{o}}\zeta}{\mu}E_x = \mu_e E_x \tag{1}$$

where u_{slip} (m s^{-1}) is the slip velocity, E_x (V m^{-1}) is the electrical field, ε_r the solution dielectric constant, ε_o (C^2 N^{-1} m^{-2}) is the vacuum permittivity, μ (kg m^{-1} s^{-1}) is the viscosity of the solution, ζ (V) is the zeta potential which is the electric potential at the shear plane separating the mobile and immobile regions of the EDL, and μ_e (m^2 s^{-1} V^{-1}) is the proportionality factor known as the electroosmotic mobility. For most microfluidic applications the thickness of the EDL is several orders of magnitude smaller than the channel and the velocity variation in the EDL can be ignored. Under these conditions, the slip velocity is also the area average velocity in the channel. Several parameters affect the average electroosmotic velocity for a given solid–liquid interface such as the wall surface charge density, ionic concentration, fluid properties, temperature, and pH of the solution

(Kirby and Hasselbrink 2004a, b; Venditti et al. 2006). Those factors related to the surface-liquid chemistry are grouped into the zeta potential. Consequently, the zeta potential is the most important parameter that defines the average electroosmotic velocity for a specific surface-liquid pairing. To this end several methods have been developed by the research community to measure zeta potential. These techniques include the current monitoring method (Arulanandam and Li 2000; Huang et al. 1988; Pittman et al. 2003; Ren et al. 2001, 2002; Rodriguez and Chandrasekhar 2005; Sinton et al. 2002; Venditti et al. 2006), streaming potential method (Erickson et al. 2000; Scales et al. 1992; Sze et al. 2003), and direct flow field measurements using fluorescent visualization or micro particle image velocimetry (Hsieh et al. 2006; Pittman et al. 2003; Sinton et al. 2002; Yan et al. 2006).

Among the microfluidics community, the most often adopted technique is the current monitoring method due to its relative simplicity and low experimental cost. In this method, the average electroosmotic velocity is measured by monitoring the current change as the test solution is displaced by a similar solution of slightly different concentration in a microchannel. By measuring the time of displacement and the channel length, the average velocity can be determined. The electroosmotic mobility or zeta potential can then be inferred from the Helmholtz-Smoluchowski slip velocity. Several researchers have applied the current monitoring method to measure zeta potential in silica and glass capillaries (Huang et al. 1988), rectangular glass microchannels (Pittman et al. 2003; Rodriguez and Chandrasekhar 2005) and polymer microchannels (Ren et al. 2001). The method has been validated by comparing results with that obtained from direct flow field measurements (Pittman et al. 2003; Sinton et al. 2002).

However, there have been a number of issues observed when applying the conventional current monitoring method (using one straight channel) in chip format devices. For instance, reservoirs in most poly(dimethylsiloxane) (PDMS) chips are formed by punching holes in the PDMS substrate which only hold a small volume of fluid. This small volume of fluid is susceptible to detrimental effects caused by electrolysis occurring at the electrodes during electroosmotic flow (Bello 1996; Macka et al. 1998; Rodriguez and Chandrasekhar 2005). Electrolysis generates hydrogen and oxygen gas bubbles as well as additional H^+ (anode) and OH^- (cathode) in the solution. The generation of these ions causes dynamic changes in the pH and electrical conductivity of the test fluid which introduces large and unpredictable errors in the current monitoring method, especially for non-buffered solutions (Bello 1996; Macka et al. 1998; Rodriguez and Chandrasekhar 2005). PDMS is also a good insulator, so a large current draw may lead to excessive Joule heating (Tang et al. 2007; Xuan 2008). Many fluid properties such as the viscosity, dielectric constant and conductivity are temperature dependent. In fact, for some solutions even the zeta potential was found to be temperature dependent (Venditti et al. 2006). Therefore, Joule heating must be controlled or reduced to minimize errors in the zeta potential measurements.

Another common issue with EOF in microchannels is the presence of undesired pressure driven flow caused by slight differences in liquid levels or meniscus shapes (Laplace pressure) between reservoirs (Sun et al. 2007; Yan et al. 2007). In situations where larger microchannels are used ($\sim 100 \times 100$ μm) and moderate pressure differences exist (100 Pa), the magnitude of the undesired pressure driven flow is often comparable or even exceeds the desired EOF. The presence of undesired pressure driven flow will distort the average velocity measured using the current monitoring method resulting in incorrect zeta potential evaluations. The influence of undesired pressure driven flow can be reduced by properly designing microchannels for EOF.

The nature of the current monitoring method also requires continues interaction with the hardware and experimental setup. For each displacement the solutions must be replaced and the electrodes must be repositioned manually. Moreover, the complete removal of the solution at the reservoir is important in order to obtain a well defined interface with sharp start and end transitions. If the reservoirs are not properly evacuated, a large mixing region can occur which makes it difficult to determine the average velocity from the current–time relationship. Due to this fact, the current monitoring experiment is usually repeated several times before a successful displacement is obtained for analysis.

To address these deficiencies, a new Y-channel chip design was proposed that improves the overall throughput and accuracy of the current monitoring method. The design allows for many displacements to be performed quickly, without replacing solutions in the reservoirs or adjusting the experimental setup. When designing the channel network special attention was paid to reduce errors caused by electrolysis, Joule heating and undesired pressure-driven flow. The Y-channel design was first validated by comparing results against other published straight channel measurements. Results are presented for zeta potential and surface conductance measurements for several biological buffers relevant to the microfluidics community in plasma treated PDMS/PDMS (P/P) and PDMS/Glass (P/G) channels. An improvement to the slope based analysis is also presented and compared to the standard total length method. Many of these results are compiled from more than 50 displacements obtained with the Y-channel design, a significant amount, compared to the quantity of displacements usually presented in literature for the current monitoring experiment.

2 Theory

2.1 Principle of operation

The proposed design consists of two side channels attached to the main displacement channel (the vertical channel) as shown in Fig. 1a. The principal of operation is as follows. One source reservoir (R1) contains the high concentration solution (100%) and the second reservoir (R2) contains the same solution diluted to 95%. An electric field is applied between R1 and R3 while R2 is left floating which allows the 100% solution to be pumped by EOF down the displacement channel. Assuming that the displacement channel is already filled with the 95% solution, the current draw will gradually increase due to a slight difference in conductivity between the two solutions. Once the current plateaus the displacement process is complete indicating that the 100% solution fills the displacement channel. The electric field is then applied between R2 and R3 while R1 is left floating and the 95% solution displaces the 100% solution filled in the displacement channel. The process is then repeated switching back and forth between the two reservoirs while recording the current draw.

Figure 1b presents the actual current–time plot after performing one set of displacements in the Y-channel design. There was a noticeable difference when comparing the current plot from the Y-channel to a standard straight channel result. Immediately after switching the electric field there was a sudden change (drop or rise) in the current because the side channel is already filled with the displacing fluid. In terms of the straight channel design, this is analogous to starting the experiment with the displacing solution partially through the channel. The dashed line in Fig. 1b represents the extrapolated straight channel result for the entire EOF channel ($L_{\mathrm{side}} + L_{\mathrm{displacement}}$). The slope of the current–time relationship still remains the same for both designs.

The most effective means of demonstrating the improvements offered by the Y-channel design is to compare actual current–time plots obtained using the two types of channel designs. Figure 2 shows this comparison for 1 mM KCl. When examining the straight channel plot (Fig. 2a), it is not easy to pinpoint the beginning and end of the displacement process due to the presence of gradual transitions. The Y-channel on the other hand (Fig. 2b), produces clearly defined start and end points with minimal transitions and repeatable displacements. Since the fluids do not have to be displaced in the reservoirs for the Y-channel, a number of displacements can be efficiently performed in a short time. It should be noted that with the straight channel it is also possible to perform repeated measurements without refilling the reservoirs by switching the polarity of the electric field after each displacement. With each displacement, however, the interface region between the solutions will grow making it more difficult to obtain good current–time plots.

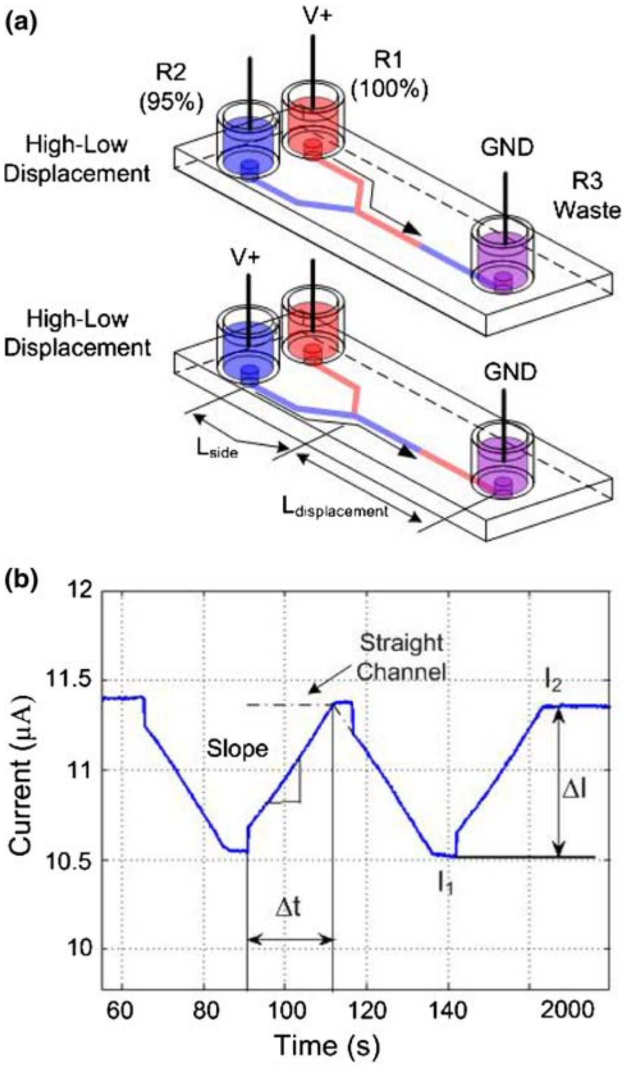

Fig. 1 **a** A schematic describing of the operation of the Y-channel design with the current monitoring method. **b** Actual current–time plot obtained for 1XTBE during experiments with notations added to explain the calculation of the zeta potential from the total length and slope methods

Long term studies of continuous EOF can also be performed in the Y-channel to estimate the operational lifetime of a given solution for a specific set of working conditions (eg. applied electric field, current draw or reservoir volume). As an example, consider Fig. 3 which shows the effect of long-term EOF operation on 10 mM KCl with 100 μl reservoirs. For most of the experiment the displacements were repeatable until about 25 min where the current fluctuates significantly. These would be attributed to bubbles formed around the electrodes and changes in the pH and electric conductivity. In this experiment the original pH of the 10 mM KCl solution was 6.83 in all three reservoirs, by the end however, the pH changed to 3.5

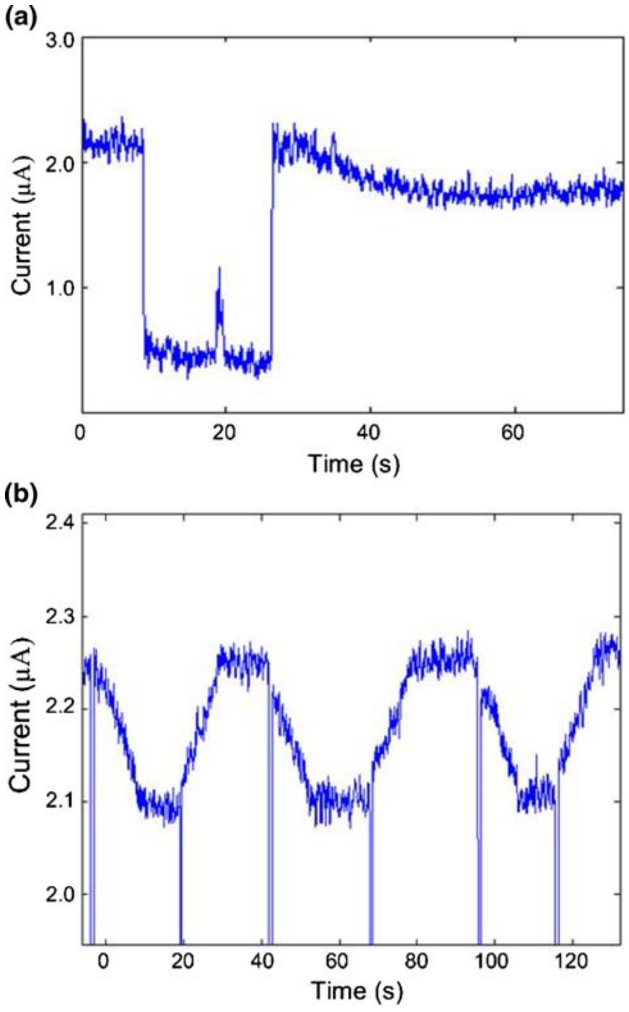

Fig. 2 Results from experiments with 1 mM KCl in **a** straight channel, and **b** Y-channel design

in R1 and R2 and 10.4 in R3. A small rise in current could also be seen with each subsequent displacement. This example demonstrated that the Y-channel is a useful tool that can provide insight into the performance of the test solution under intended operating conditions.

2.2 Channel network and chip design

When designing the Y-channel proper consideration was given to the various factors which may affect the zeta potential measurement using the current monitoring method. As stated before, these factors include undesired pressure driven flow, electrolysis and Joule heating.

Undesired pressure driven flow can be suppressed by increasing the hydrodynamic resistance of the microchannel through a reduction in channel height $\left(R_h = 12\mu l/(wh^3)\right)$ (Sun et al. 2007; Yan et al 2007). Reducing the channel height to about 5–10 μm eliminates the majority of unwanted pressure driven flow. It should be noted that a lower limit exists for the channel height where the EDL thickness becomes comparable to the channel height and the Helmholtz-Smoluchowski equation becomes invalid (Masliyah and Bhattacharjee 2006). A practical consideration also exists since the current draw must be large enough so that it can be measured by the experimental setup. The magnitude of the current draw can be controlled by the width of the microchannel. Since the extent of Joule heating and electrolysis depends on the current draw the width also has an upper limit. Consequently, a number of configurations for the Y-channel design are required to test the various fluids which are listed in Table 1. Choosing the appropriate arrangement depends on the conductivity and estimated EDL thickness of the test fluid. The procedure is discussed further in the experimental section.

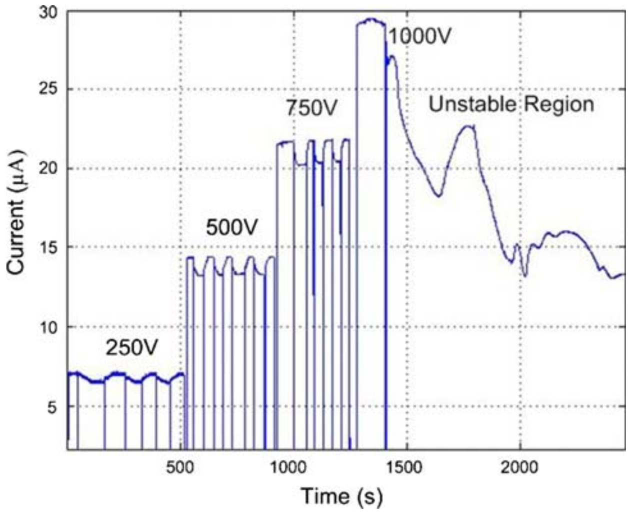

Fig. 3 Long-term current–time plot for 10 mM KCl displaced at several applied electric fields. The volume of the test fluid was only 100 μl which results in eventual instability in the current monitoring due to the accumulation of electrolysis byproducts

Several measures were taken to further reduce electrolysis effects. Large reservoirs (1.5 ml) were used in the experiments to absorb the byproducts of electrolysis and operating times were reduced for non-buffered solutions. In

Table 1 Average channel dimensions of all silicon masters used in fabricating Y-channel chips for electroosmotic mobility measurements

Master No.	Average width (μm)	Average height (μm)
Y–500–2	483.33	9.06
Y–500–3	490.00	7.11
Y–200–1	192.83	10.37
Y–200–2	192.50	5.82
Y–200–3	192.25	7.00
Y–100–1	94.75	5.76
Y–100–2	94.12	7.32

addition, platinum electrodes were placed far from the entrance of the channel to increase the time it takes for electrolysis byproducts to diffuse into the microchannel. Large reservoirs also reduce Laplace pressure effects by minimizing the shape of the meniscus.

A potential negative aspect of the Y-channel design is that any asymmetry in the side channels will alter the uniformity of the electric field in the displacement channel. An inequality may exist between the two side channels due to manufacturing defects or particle blockage. Shorter side channels will have a lower impact on the displacement process since they represent a small portion of the total resistance of the electric field ($R_T = R_{\text{side}} + R_{\text{displacement}}$). Thus shorter side channels are favorable but the suppression of undesired pressure driven flow must still be considered. In this study a ratio of 1:4 was chosen for the side and displacement channels. The length of the displacement channel is also important for the current monitoring method. The shorter the channel the larger the error in determining the displacement time while a longer channel will require excessive voltages to be applied to achieve a reasonable displacement time.

After considering all of the above mentioned factors a series of channel designs were fabricated with the following dimensions. The displacement channel and side channel lengths are 4 and 1 cm, respectively. The side channels intersect the displacement channel at a 45° angle and 50 μm fillets are applied to the corners to eliminate high local variation of electric field. The channel height ranges between 5 and 9 μm with widths of 100, 200 and 500 μm. For the case of 9 × 500 μm channels, a 1 cm head difference between reservoirs R1 and R2 (least resistance path) results in a flow rate of 9.11×10^{-3} μl/min. An applied voltage of 1,000 V between R1 and R3 and an exceptionally low zeta potential of −10 mV creates an EOF flow of 0.306 μl/min. Thus the error caused by undesired pressure driven flow is only 3% of the EOF flow which is well within the uncertainties expected from the measurement system.

2.3 Current–time analysis

Determining the zeta potential from the current–time plot for the Y-channel design required a slight modification to the original techniques based on the straight channel. To explain the process of calculating the zeta potential from the current–time plot, an actual plot obtained for 1XTBE in a P/G chip (Fig. 1b) was used. Two techniques exist for calculating the average electroosmotic velocity from the current–time plot: the total length method and the slope method. The most straightforward is the total length method where the velocity is estimated from the displacement length, $L_{\text{displacement}}$ (m) and time, Δt (s):

$$u_{av} = \frac{L_{\text{displacement}}}{\Delta t} \tag{2}$$

Note that in the Y-channel design the displacement length is the length of the displacement channel. Once the velocity is known the electroosmotic mobility or zeta potential can be calculated from the Helmholtz-Smoluchowski equation. The challenge in using Eq. (2) lies in the difficulty in determining the displacement time. Small current fluctuations and gradual transitions due to diffusive mixing at the interface can make it difficult to accurately pinpoint the start and end of the displacement process. Although the Y-channel design alleviates these problems, having a secondary analysis technique will assist in validating results.

Ren et al. (2002) developed a method to determine the electroosmotic mobility from the slope of the current–time plot. The method uses the fact that for small concentration differences the change in current is linear. The derived equation for the electroosmotic mobility given by Ren et al. (2002) for a straight channel is:

$$\mu_{eo} = \frac{\text{slope} \cdot L_{\text{channel}}}{E_x^2 \cdot \mathbf{A}_{\text{c}}} \cdot \frac{1}{\Delta\lambda_b} \tag{3}$$

where the slope is the current change per time change (A/s), L_{channel} (m) is the total channel length, $\Delta\lambda_b$ (S/m) bulk conductivity difference between the solutions, and A_c (m^2) is cross sectional area of the microchannel.

Equation (3) was used initially in this study to evaluate the electroosmotic mobility. After performing a number of preliminary experiments, however, a significant disagreement was seen in the results obtained from the total length and slope methods. The reason for this discrepancy lies in the bulk conductivity term, $1/\Delta\lambda_b$, used in Eq. (3). In most cases, the bulk conductivity difference was measured to be around $\Delta\lambda_b = 5\%$; however, the actual current difference obtained from the current–time plot was often between 6 and 8%. This results in a miscalculation of the electroosmotic mobility due to the inequality between the slope and conductivity difference. The cause of this error can be attributed to a number of factors involved in measuring the bulk conductivity difference.

The bulk conductivities of the two solutions were measured in the reservoirs prior to performing an experiment. These measurements, however, may not represent the actual conductivities of the solutions in the channel as the bulk conductivity may change due to temperature fluctuations (∼2%/°C) or electrolysis. In addition, the measurement accuracy of most conductivity meters is between 0.5 and 2% which obviously results in a large error when small differences are taken. Furthermore, in channels with high surface to volume ratios, such as those used in this work, the surface conductance may also represent a significant portion (10–20%) of the overall current (Arulanandam and

Li 2000). The analysis presented by Ren et al. (2002) omits this fact in the development of Eq. (3).

To improve the slope method, the bulk conductivity difference is replaced by the actual current difference measured at the two plateaus in the current–time plot. By incorporating the actual measured current, changes in surface conductance and bulk conductivity will be automatically included in the analysis. In addition, measuring the current with a high accuracy picoammeter is at least an order of magnitude more accurate than measuring the bulk conductivity with most probes. The modified current slope analysis for the Y-channel is then given as:

$$\mu_{eo} = \frac{\text{slope} \cdot (L_{\text{displacement}} + L_{\text{side}})}{E_x \cdot (I_2 - I_1)} \tag{4}$$

where I_1 and I_2 (A) are the current measured before and after the displacement. For the Y-channel the electric field is also defined as:

$$E_x = -\frac{\Delta V}{L_{\text{displacement}} + L_{\text{side}}}. \tag{5}$$

For all experiments both the total length method and the modified slope method were used to determine the zeta potential.

2.4 Surface conductance

In addition to zeta potential, the surface conductance of a solid–liquid interface can also be determined from the current monitoring method (Arulanandam and Li 2000). Surface conductance arises from the presence of the EDL as the surplus of ions near the surface results in an increase in the local conductivity. Surface conductance is often modeled as a thin conducting sheet along the perimeter of the channel. Thus for channels with larger surface area to volume ratios, the current carried by the surface conductance may be significant. In the streaming potential method the surface conductance must be taken into account or measurements will lead to inaccuracies in determining the zeta potential (Masliyah and Bhattacharjee 2006). Therefore, surface conductance is an important parameter of EOF, especially in shallow channels, and should also be measured.

In steady EOF the total current is composed of the bulk, surface and convection (fluid flow) currents. The convection current is several orders of magnitude smaller than the other two currents and can be neglected (Masliyah and Bhattacharjee 2006). The total current reduces to:

$$I_{\text{total}} = I_{\text{bulk\_cond}} + I_{\text{surf\_cond}} = \lambda_b A_{\text{cross}} E + \lambda_s P E \tag{6}$$

where λ_b (S/m) is the solution bulk conductivity, A_{cross} (m^2) is the cross sectional area of the microchannel, λ_s (S) is the surface conductance, P (m) is the perimeter, and E (V/m) is the applied electrical field. By first measuring the bulk conductivity of the solution the surface conductance can be determined by rearranging Eq. (6),

$$\lambda_s = \frac{I_{\text{measured}}}{EP} - \frac{\lambda_b A_{\text{cross}}}{P} \tag{7}$$

where I_{measured} is the steady current recorded during electroosmotic flow in a microchannel. In the above equation one may also account for the variation in bulk conductivity due to the presence of the EDL (Arulanandam and Li 2000). However, this implies knowledge of the structure of the EDL which is difficult to determine for the complex solutions that were tested. Thus the variation of the bulk conductivity was neglected in the measurement of the surface conductivity. The Y-channel was also used to determine the surface conductance of the solutions where the two source reservoirs were filled with the same solution and the current was monitored while alternating the electric field.

3 Materials and experimentals

3.1 Chemicals

Buffer and electrolyte solutions tested included: 10 and 1 mM KCL (EM Science), 1X TAE (Tris base, glacial acetic acid and EDTA (BDH)), 1X TBE (Tris base, EDTA (BDH), boric acid (Sigma Aldrich)), 10X MOPS (BioShop, Canada Inc), 10 mM HEPES (Sigma Aldrich) and 10X PBS (Fisher Scientific). Before each test all solutions were prepared and filtered. Channel masters were fabricated from SU-8 2005 and SU-8 2015 photoresist (MicroChem. Corp., Newton, MA) using soft lithography technology. Replica molds of PDMS were poured from Sylgard 184 in a ratio of 10:1 base to curing agent (Dow Corning, San Diego, CA).

3.2 Microfluidic chip fabrication

PDMS chips with the Y-channel configuration were fabricated using standard soft lithography technology. In order to accommodate the various solutions to be tested, several silicon masters were fabricated with various channel heights and widths as summarized in Table 1. The channel features on the masters were measured with a contact profilometer (Mitutoyo SJ-400) to ensure channel uniformity and experimental repeatability. The fabricated PDMS microchannels were then air plasma treated (Harrick Plasma, Ithaca NY) at 29.6 W for 40 s and bonded either to a microscope glass slide or a PDMS coated microscope glass slide. PDMS coated microscope slides were fabricated by spincoating 1 ml of PDMS (10:1) at 3,000 rpm for 30 s to achieve a 30 μm layer. Ultra pure water was introduced into the channels after bonding and glass reservoirs (1.5 ml) were mounted using liquid PDMS to make a leak-proof attachment. The filled channels were left for two days to allow for the zeta potential to stabilize before performing current monitoring experiments (Choi 2007; Ren et al. 2001). An image of a complete chip is shown in Fig. 4a.

3.3 Experimental setup

A schematic of the experimental setup is presented in Fig. 4b. A high voltage power supply (SL10, Spellman) is connected to an electrical circuit containing a switch that distributes the applied voltage via platinum wires to the reservoirs. The electrical switch is used to quickly switch the applied voltage between the two reservoirs R1, R2 while R3 is kept grounded. A custom chip holder was built to attach the electric circuit and to fix the microfluidic chip in place. The current was measured with a picoammeter (Keithley 6485) connected in series with the chip. The applied voltage and current were exported from the power supply and picoammeter and recorded through a DAQ (NI-PCI-6221, National Instruments) using a custom made LabVIEW program. The ambient temperature was monitored with a standard K-type thermocouple. A 10 W AC fan was placed beside the chip to maintain the chip at room temperature. To calculate the zeta potential and surface conductance from the current–time plots a custom Matlab program was written.

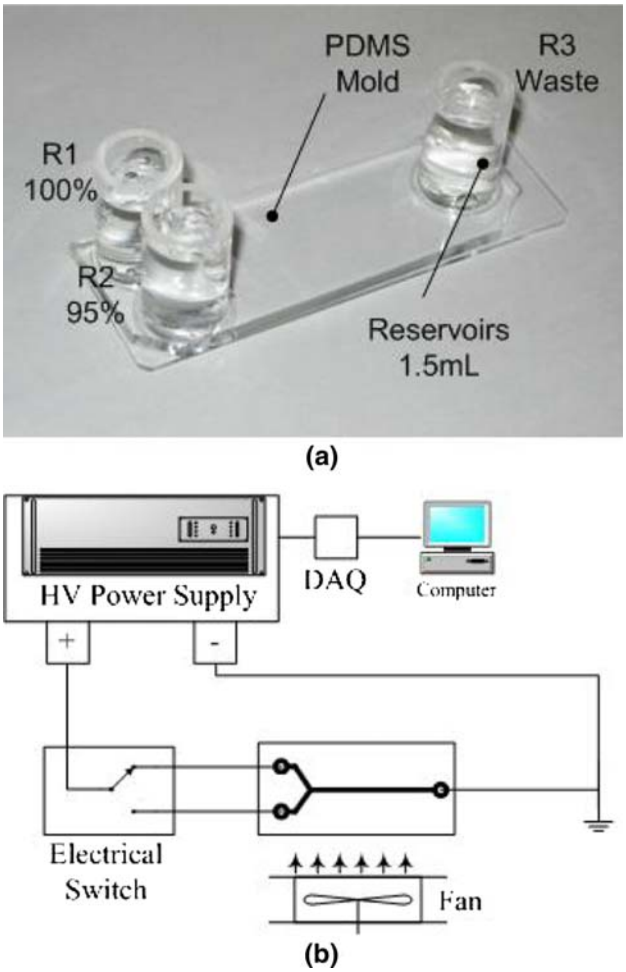

Fig. 4 **a** Image of completed PDMS chip with attached reservoirs. **b** Experimental setup used for the current monitoring method and application of the Y-channel design

Also, a fluorescent microscopy setup was used to visualize the electroosmotic flow during the switch processes between the source reservoirs. An inverted microscope (GX-71, Olympus) with a blue light filter and a 1,392 × 1,040 pixels CCD camera (CoolSNAP ES, Photometrics) was used to visualize a pumped dyed solution form one branch of the Y channel design. A halogen lamb was used to illuminate the flow which contained the fluorescein dye (Molecular Probes).

3.4 Experimental procedure

For each new test solution, the bulk conductivity and pH were measured for both solutions prior to performing any experiments. Measurements were performed using high-accuracy, low-sample-volume electrodes (MI-915, MI-4154 Microelectrodes Inc Bedford, USA) combined with a pH/conductivity meter (Orion 5 Star, Thermo Electron Corp.). In the performed experiments the current draw was limited to a range of 2–10 μA. The first step in performing an experiment was to select the appropriate Y-channel design that fits the desired 2–10 μA current draw. Using the measured conductivity the required channel cross-section area was calculated ($A_c = IL_{\text{channel}}/V\lambda_b$). Then a master which agrees with the calculated area was chosen from Table 1 to fabricate the test chip.

Once the solutions were properly prepared and the chip was placed in the holder the first step was to validate the symmetry of the fabricated chip. This was done by filling all the reservoirs with the 100% solution and recording the steady state current as the solution was pumped from R1 to R3 and R2 to R3. If the two currents were identical the chip was confirmed to be symmetric and can be used for zeta potential measurements. Then the fluid in R2 was displaced with the 95% solution and the conductivity and pH were recorded in all three reservoirs. All reservoirs were filled to the same level to prevent any pressure driven flow. The electric field is then applied from R2 and R3 until full displacement was achieved by reaching a new current plateau. Afterwards, the electric field was then alternated between the two solutions several times to obtain a desired number of displacements. After a set of switches were completed, the pH, conductivity and temperature of the solutions in all three reservoirs were measured again. A typical current monitoring experiment involved 4 switches at 4 different applied voltages resulting in a total of 16 displacements.

As mentioned previously, the current time plots shown in Figs. 2 and 3 revealed that the Y-channel design provides more reliable and stable displacements for analysis than the conventional straight channel design. To further investigate the performance of the Y-channel the switching process was also studied using fluorescence microscopy. In this experiment, the first source reservoir (R1) was filled with a pure 1X TAE buffer while the second source reservoir (R2) was filled with a 1X TAE buffer solution with addition of 10 mM fluorescein dye. A series of images showing the switching process for two alternating displacements are presented in Fig. 5. From the sequence of images it is clear that the Y-channel produces a sharp interface and complete displacement of the solution in the displacement channel was attained.

In Fig. 5 a small amount of the displacing fluid appears in the other side channel during the displacement process. This transport of displacing fluid was attributed to diffusion caused by the high concentration difference between the dyed and non-dyed solution. If there was a significant amount of backflow a greater amount of sample leakage would be expected. In an actual test, a small amount of diffusion would also be expected for the 100 and 95% solutions. To address this issue a larger uncertainty (1%) was added to the displacement length when calculating the zeta potential.

An uncertainty analysis was performed for all zeta potential calculations using the least squares method for a confidence level of 90%. The bias uncertainty of the measurement devices were taken from literature published by the manufacturers: voltage (5 V), current (0.1%), conductivity (0.5%), channel length (1%), channel width (0.1%), channel height (0.1%), and displacement time 1 s. The random uncertainties in measuring the current and voltage were taken as the standard deviation of the actual readings. The uncertainty propagation of a variable in the calculation of the zeta potential was determined in the same approach as presented by Beckwith et al. (1993).

4 Results and discussion

4.1 Y-channel design validation

In order to validate the zeta potential measurements obtained with the Y-channel design, results were compared to published data obtained using conventional straight microchannels as summarized in Table 2. Also included in the comparison the result for 50 mM $NaHCO_3/Na_2CO_3$ obtained with both the Y-channel and straight channel designs. The comparison shows a good agreement between results as most discrepancies are within 3–4%. However, for 10 mM KCl there is a larger discrepancy, around 10% for P/G channels, and 23% for P/P channels. The most likely cause is a difference in fabrication methods, most notably plasma treatment conditions.

It is well known that the surface charge generated by plasma treatment decays quickly in PDMS before it stabilizes (Choi 2007; Ren et al. 2001). During this process the electroosmotic mobility or the zeta potential can decrease significantly and therefore it is important to know the time between treatment and testing when performing a comparison. In this study, the chips were plasma treated for 40 s at 29.6 W, filled with de-ionized water and used to perform experiments after waiting for 2 days. Unfortunately, most studies do not report the exact waiting period which makes it difficult to compare results. In spite of these facts, the Y-channel results show good agreement with many published results which assures confidence in the accuracy of Y-channel zeta potential measurements.

4.2 Measuring the zeta potential of various solutions

The Y-channel design was applied to measure the zeta potential of a number of solutions commonly used amongst the microfluidics community (KCl, TAE, TBE, TE, MOPS, HEPES and PBS). Tests were performed in P/P channels and P/G to study the influence of channel material combinations on EOF. Figure 6 summarizes the results of these experiments for the various solutions and channel material

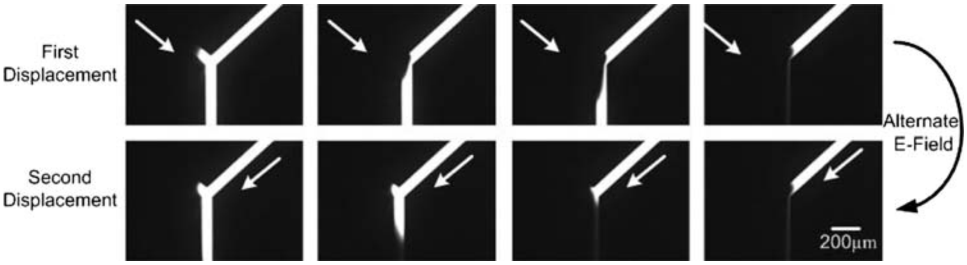

Fig. 5 Sequence of images obtained with fluorescence microscopy for the displacement process. Fluorescein dye (100 µM) was added to one stream in the Y-channel to study the switching process. The images show one set of alternating displacements between the dyed and non-dyed fluid

Table 2 Zeta potential results from the straight channel and Y-channel design calculated with the total length method Eq. (2)

Solution	Channel format	Zeta potential, ζ (mV) straight channel	Zeta potential, ζ (mV) Y-Channel
50 mM $NaHCO_3$/Na_2CO_3	P/G	–59.12[a]	–56.79
1 mM KCl	P/G	−88.32[b]	−92.26 ± 4.63
	P/P	−87.00[c]	−83.34 ± 3.87
10 mM KCl	P/G	−54.84[b]	−49.89 ± 1.45
	P/P	−37.57[b]	−49.11 ± 1.63
1X TE	P/G	−68.13[b]	−66.09 ± 3.67
1X TBE	P/G	−48.05[b]	−49.19 ± 1.30

[a] Current monitoring experiments performed in the lab

[b] Results published by Venditti et al. (2006)

[c] Results published by Sze et al. (2003)

combinations. Zeta potential values calculated using both the total length and modified slope methods are included in the plot. Each data point in Fig. 6 represents an average zeta potential compiled from analyzing a minimum of 50 displacements for a particular solution.

Results clearly indicate that the zeta potential determined using the total length method and the modified slope method are in good agreement. Over the entire set of results the discrepancy between the two methods is less than 6.8%, which is within the experimental uncertainties of the measurements. Since many microfluidic devices are fabricated in either P/P or P/G configurations, it is important to characterize the zeta potential for each solution in both situations. The electroosmotic mobility of a hybrid microchannel can be approximated by a weighted average of the electroosmotic mobilities of the two materials (Bianchi et al. 2001). The results presented in Fig. 6 show similar zeta potential values for both type of microchannels. Given the channel dimensions used in this study (100–500 µm width, 5–9 µm height), both the PDMS and glass contribute almost equally to the average electroosmotic mobility of the hybrid microchannel. This indicates that the plasma treatment used to fabricate the microchannels alters the PDMS surface to give it electrokinetic properties similar to glass. This result disagrees with several reports that indicate lower zeta potential in P/P devices (Bianchi et al. 2001; Venditti et al. 2006) and agrees with others (Ren et al. 2001). The reason for this discrepancy is not entirely clear, but may be attributed to differences in fabrication of the P/P devices, particularly the curing time of PDMS and plasma treatment conditions.

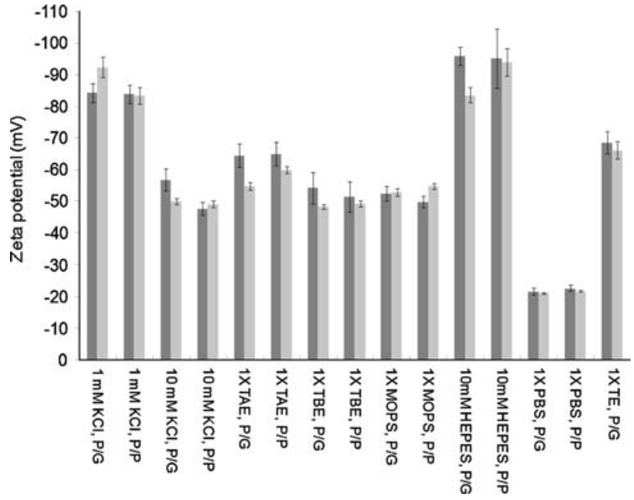

Fig. 6 Zeta potential measured using the Y-channel design for various fluids in PDMS/PDMS (P/P) and PDMS/Glass (P/G) chips. *Dark* columns are for calculations using the slope method and *light* columns the total length method. *Error bars* represent a 90% confidence level

4.3 Surface conductance measurements

Experiments were performed with the Y-channel design to estimate the surface conductivity of several solutions and to study parameters that may affect surface conductivity including the applied electric field strength and substrate material. Figure 7a shows the measured surface conductivity for 1XTAE buffer (dark bars) and 10 mM KCl solution (medium bars) in a P/P microchannel under several applied electric fields. The results indicate a slight trend where surface conductivity increases with applied electric field strength. However, theory suggests that the surface conductance is a property of the electric double layer and should not be affected by an externally applied electric field (Masliyah and Bhattacharjee 2006). In this work the apparent increase in surface conductivity is actually attributed to the inherent difficulty in measuring the solution bulk conductivity.

Obtaining accurate measurements of the surface conductivity proved to be difficult due to the sensitivity of Eq. (7) to experimental uncertainties. The calculation contains a subtraction operation which causes the largest uncertainty propagation of all mathematical operations (Beckwith et al. 1993). For instance, consider the effect the measured bulk conductivity has on the calculated surface conductivity. Figure 7a also presents the results for 10 mM KCl where the surface conductivity was calculated from the bulk conductivity measured at the end of the experiment (light bars) as opposed to the beginning of the experiment (medium bars). Over the time of the experiment (7 min), the bulk conductivity changed from $\lambda_b = 1{,}301$ µS/cm to $\lambda_b = 1{,}315$ µS/cm, about a 1% difference.

The bulk conductivity increase may have been caused by a slight temperature rise or more likely the addition of extra ions from electrolysis. The propagation of this small change is severe in determining the surface conductivity. The 1% increase bulk conductivity results in a 15% difference between the surface conductivity calculated using the beginning (medium bars) and final (light bars) bulk conductivities, as seen in Fig. 7a. With this fact in mind, the slight increase in apparent surface conductivity can be accounted for by the increase in overall bulk conductivity. The results for the first measurement of surface conductivity with the beginning bulk conductivity (medium bar at 20 kV/m) compares well with the last measurement calculated with the ending bulk conductivity (light bar at 40 kV/m). Therefore, it is probable that the surface conductivity is actually independent of the applied electric field as expected. The example illustrates the difficulty in acquiring surface conductivity estimations and should be considered when using the results presented here.

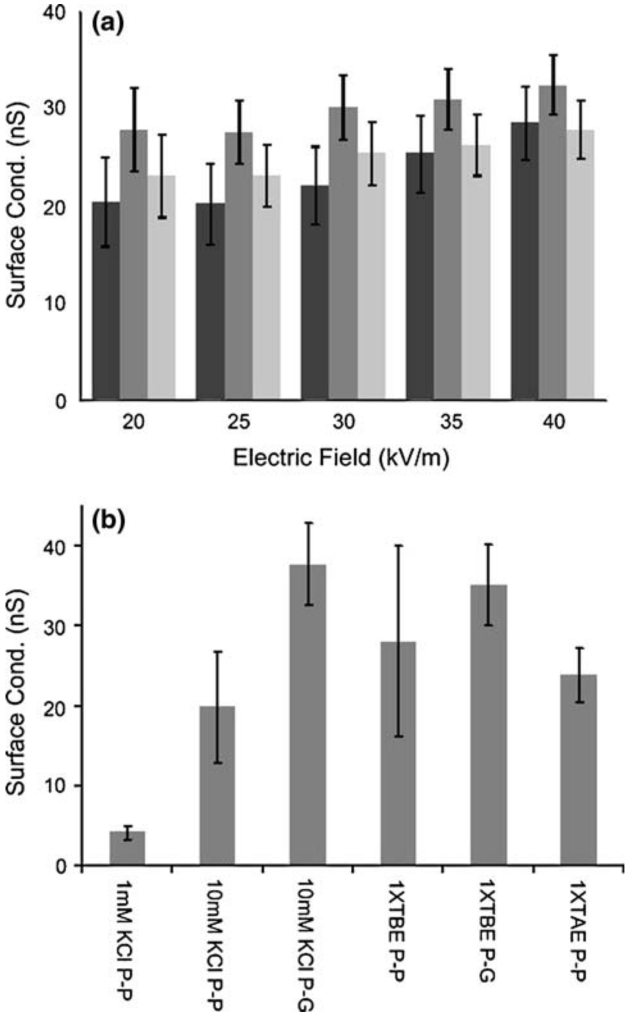

Fig. 7 **a** Surface conductance dependence with the electric field for PDMS-PDMS microchannels. *Dark pattern* is for 1X TAE buffer, *medium pattern* 10 mM KCl by using the solution conductivity at the start of the experiment and *light* 10 mM KCl by using the solution conductivity at the end of the experiment. **b** Surface conductance of different solutions for P–P and P–G microchannels each value represents the average of 20 measurements

Results for the average surface conductivity for various solutions in P/P and P/G microchannels are presented in Fig. 7b. Analyzing the results for 1 mM KCl ($\lambda_s = 4.5$ ns) and 10 mM KCl ($\lambda_s = 19.8$ ns) the surface conductivity increases with higher concentrations as would be expected. However, unlike the bulk conductivity the surface conductivity does not increase proportionally with ionic concentration ($\lambda_b = 141$ μs/cm for 1 mM KCl and $\lambda_b = 1{,}441$ μs/cm for 10 mM KCl). Again this condition is expected since the surface conductivity depends on the concentration of ions as well as their arrangement in the electric double layer (Masliyah and Bhattacharjee 2006). For the shallow microchannels used in this study the surface current represented approximately 10–15% of the total measured current which suggests that the surface conductivity should not be ignored when modeling EOF in shallow microchannels.

Of greater interest are the results for the same solution in the hybrid microchannels. For both 10 mM KCl and 1XTBE the surface conductivity is significantly larger in P/G than in P/P microchannels indicating that the glass electric double layer carries a much larger current than the PDMS. This is opposite to the zeta potential measurements where the electric double layer conditions were found to be similar. However, a clear and quantitative explanation for this discrepancy cannot be provided through this study using only the current data. A more thorough investigation is recommended using other measurement techniques and theoretical models to probe the properties of the electric double layer and surface conductivity.

5 Summary

This study aims to improve the accuracy of the zeta potential measurement using the current monitoring method by developing a new chip design. A Y-channel configuration is presented here that increases the throughput and stability of the displacement process. The Y-channel generates sharper start and end transitions with excellent linearity in the current–time relationship compared to the conventional straight channel configuration. Induced pressure driven flow, electrolysis and Joule heating influences were minimized through the proper design of the microchannel dimensions. In comparison to data available in literature, the zeta potential measurements using the Y-channel design showed good agreement across a number of solutions. In addition, the zeta potential measurements for a variety of solutions commonly used in microfluidic devices are reported. The results showed that plasma treated PDMS/PDMS and PDMS/Glass microchannels possessed similar zeta potentials. Calculations using the total length method and the modified slope method introduced in this work were also in good agreement.

In this study the surface conductivity was also investigated and measurements are reported for several solutions. Results show that the surface conductivity does not depend on the applied electric field and unlike the zeta potential, a significant difference was found between PDMS/PDMS and PDMS/Glass microchannels. In the shallow channels used in this study the surface conductance current typically accounted for 10–15% of the total current. However, the surface conductivity measurements are subject to a great deal of uncertainty due to the nature of the calculations and should be considered qualitatively. Further investigations are needed to effectively quantify the parameters affecting surface conductivity. As evidence by the results presented in this paper, the Y-channel design provides a significant improvement in the quality and accuracy of the current monitoring method.

Acknowledgments The authors gratefully acknowledge the support of research grants of the Natural Sciences and Engineering Research Council (NSERC) of Canada to C. L. Ren and D. A. Johnson, the Department of Mechanical Engineering at King Saud University for sponsoring Zeyad Almutairi and Ontario Graduate Scholarship and Canada Graduate Scholarship to Tomasz Glawdel. Zeyad Almutairi and Tomasz Glawdel made equally contributions to this study.

References

Arulanandam S, Li DQ (2000) Determining zeta potential and surface conductance by monitoring the current in electro-osmotic flow. J Colloid Interface Sci 225:421–428

Beckwith TG, Marangoni RD, Lienhard JH (1993) Mechanical measurements, 5th edn. Prentice Hall

Bello MS (1996) Electrolytic modification of a buffer during a capillary electrophoresis run. J Chromatogr A 744:81–91

Bianchi F, Wagner F, Hoffmann P, Girault HH (2001) Electroosmotic flow in composite microchannels and implications in microcapillary electrophoresis systems. Anal Chem 73:829–836

Chen CH, Santiago JG (2002) A planar electroosmotic micropump. J Microelectromech Syst 11:672–683

Choi ES (2007) Improvement of electroosmotic flow characteristics in poly(dimethylsiloxane) channels via a long life chemical surface modification. In: 7th international conference on miniaturized chemical and biochemical analysis systems, 5–9 October 2007, CA, USA

Erickson D, Li DQ, Werner C (2000) An improved method of determining the zeta-potential and surface conductance. J Colloid Interface Sci 232:186–197

Fluri K, Fitzpatrick G, Chiem N, Harrison DJ (1996) Integrated capillary electrophoresis devices with an efficient postcolumn reactor in planar quartz and glass chips. Anal Chem 68:4285–4290

Gravesen P, Branebjerg J, Jensen OS (1993) Microfluidics—a review. J Micromech Microeng 3:168–182

Harrison DJ, Manz A, Fan ZH, Ludi H, Widmer HM (1992) Capillary electrophoresis and sample injection systems integrated on planar glass chip. Anal Chem 64:1926–1932

Hsieh SS, Lin HC, Lin CY (2006) Electroosmotic flow velocity measurements in a square microchannel. Colloid Polym Sci 284:1275–1286

Huang XH, Gordon MJ, Zare RN (1988) Current-monitoring method for measuring the electroosmotic flow rate in capillary zone electrophoresis. Anal Chem 60:1837–1838

Kirby BJ, Hasselbrink EF (2004a) Zeta potential of microfluidic substrates: 1. Theory, experimental techniques and effects on separations 25:187–202

Kirby BJ, Hasselbrink EF (2004b) Zeta potential of microfluidic substrates: 2. Data for polymers. 25:203–213

Macka M, Andersson P, Haddad PR (1998) Changes in electrolyte pH due to electrolysis during capillary zone electrophoresis. Anal Chem 70:743–749

Masliyah J, Bhattacharjee S (2006) Electrokinetic and colloid transport phenomena, Wiley

Pittman JL, Henry CS, Gilman SD (2003) Experimental studies of electroosmotic flow dynamics in microfabricated devices during current monitoring experiments. Anal Chem 75:361–370

Ren XQ, Bachman M, Sims C, Li GP, Allbritton N (2001) Electroosmotic properties of microfluidic channels composed of poly(dimethylsiloxane). J Chromatogr B 762:117–125

Ren LQ, Escobedo-Canseco C, Li DQ (2002) A new method of evaluating the average electro-osmotic velocity in microchannels. J Colloid Interface Sci 250:238–242

Rodriguez I, Chandrasekhar N (2005) Experimental study and numerical estimation of current changes in electroosmotically pumped microfluidic devices. Electrophoresis 26:1114–1121

Scales PJ, Grieser F, Healy TW, White LR, Chan DYC (1992) Eelectrokinetics of the silica solution interface—a flat-plate streaming potential study. Langmuir 8:965–974

Sinton D, Escobedo-Canseco C, Ren LQ, Li DQ (2002) Direct and indirect electroosmotic flow velocity measurements in microchannels. J Colloid Interface Sci 254:184–189

Sun Y, Lim CS, Liu AQ, Ayi TC, Yap PH (2007) Design simulation and experiment of electroosmotic microfluidic chip for cell sorting. 133:340–348

Sze A, Erickson D, Ren LQ, Li DQ (2003) Zeta-potential measurement using the Smoluchowski equation and the slope of the current-time relationship in electroosmotic flow. J Colloid Interface Sci 261:402–410

Tang G, Yan D, Yang C, Gong H, Chai C, Lam Y (2007) Joule heating and its effects on electrokinetic transport of solutes in rectangular microchannels. Sens Actuators A 139:221–232

Venditti R, Xuan XC, Li DQ (2006) Experimental characterization of the temperature dependence of zeta potential and its effect on electroosmotic flow velocity in microchannels. Microfluid Nanofluid 2:493–499

Xuan X (2008) Joule heating in electrokinetic flow. Electrophoresis 29:33–43

Yan DG, Yang C, Nguyen NT, Huang XY (2006) A method for simultaneously determining the zeta potentials of the channel surface and the tracer particles using microparticle image velocimetry technique. Electrophoresis 27:620–627

Yan DG, Yang C, Huang XY (2007) Effect of finite reservoir size on electroosmotic flow in microchannels. Microfluid Nanofluid 3:333–340

Zhang JB, He GW, Liu F (2006) Electro-osmotic flow and mixing in heterogeneous microchannels. Phys Rev E 73:056305